LINKS OF THE SOUTHERN OCEAN TO THE GLOBAL CLIMATE

DIRK OLBERS
Alfred-Wegener-Institute for Polar and Marine Research, Bremerhaven, Federal Republic of Germany.

1 Introduction

Roughly 30% of the world ocean volume has temperatures below $2°C$. Paleoceanographic data have revealed that this was not always the case. Before the Drake Passage opened due to continental drift about 30 Myr BP the climate of the ocean was considerably warmer. In the course of the establishment of the Southern Ocean in its present shape the difference between surface and bottom temperatures in equatorial regions changed from about $7°C$ to its present value of about $26°C$ (Berger 1981). The polar climate of the southern hemisphere got increasingly colder by the growth of glacial ice on the Antarctic continent and the gradual development of the sea ice cover around it. Today the seasonal cycle changes the sea ice extent in the Southern Ocean from about $3 \cdot 10^6 km^2$ in austral summer to $20 \cdot 10^6 km^2$ in austral winter, an area which is roughly as big as the North Atlantic Ocean.

The general cooling of the southern high latitudes of our planet was accompanied by a corresponding development of the present cold water sphere in the entire world ocean. The production of the cold water takes place in the polar regions. The coldest and heaviest water masses - combined under the name Antarctic Bottom Water ($AABW$) - are formed in the Southern Ocean all around Antarctica, predominantly adjacent to the continent in the subpolar seas - the Weddell and Ross Seas. The formation is a consequence of a complex chain of interactions between the ocean, sea and shelf ice and the atmosphere. Ventilation processes originating from heat transfer across the air-ocean interface and brine release due to sea ice production generate meridional overturning of the world ocean which carries passive tracers such as oxygen and carbon dioxide into the deep ocean. These deep ventilation processes are believed to be responsible for the anomalously cold state of the modern ocean.

The opening of the Drake Passage also established the strongest current system in the world ocean, the Antarctic Circumpolar Current (ACC), with mass transport of roughly $130Sv$ ($1Sv = 10^6 m^3 s^{-1}$).

NATO ASI Series, Vol. I 11
Modelling Oceanic Climate Interactions
Edited by J. Willebrand and D. L. T. Anderson

Though primarily driven by the wind the *ACC* contains a strong thermohaline driven component originating from the deep-reaching convection under the sea ice. As the most important link between the ocean basins of the Atlantic, Pacific and Indian Oceans, it serves as a conduit of all active and passive tracers which affect the climate, notably heat and salt which strongly influence the oceanic mass stratification and consequently the ocean circulation, and the greenhouse gas carbon dioxide.

The strong circulation of the *ACC* acts as barrier to the meridional exchange of properties between the Southern Ocean and the oceans to the north. Unlike other oceans where the poleward transfer of heat is mainly carried by the mean geostrophic currents, the Southern Ocean circulation has to establish the heat transfer in frictional boundary layers and by transient motions. The vigorous meso-scale eddy field originating from internal instabilities of the *ACC* is the main carrier of heat poleward to the south. This meridional heat transport is intimately related to the dynamical balance of the *ACC* which can only establish the observed size of the current by downward flux of momentum due to the eddy action and subsequent loss by pressure action at submarine topography.

The remote location and the hostile climate of the Southern Ocean is mostly responsible for our lack of knowledge of many important processes which act in the area of the Southern Ocean and influence other ocean regions and ultimately our climate. Models of the sea ice cover, water mass formation and ocean circulation thus constitute an important tool to investigate and interrelate these processes. In the following we will discuss the processes involved in the heat transport across the Polar Front, the dynamical balance of the *ACC*, and formation of bottom water in the Weddell Sea. A broader view of the subject is given by Gordon (1988), Nowlin and Klinck (1986) and Whitworth III (1988).

2 The heat link: the transport of heat across the polar front

The Southern Ocean is bounded to the north by a circumpolar system of fronts, the Polar Front (*PF*) and the Subantarctic Front (*SAF*) which separate the cold Antarctic water from the warmer waters to the north. The area south of this frontal boundary is exposed to the cold polar air masses which leads to substantial cooling of the surface waters. Gordon and Owens (1987) have estimated that on average about $0.3PW$ ($1PW$ = 1Petawatt= $10^{15}W$) leave the ocean to the atmosphere in the region south of the Polar Front. This loss of heat must be compensated by a meridional net southward heat transport across the front. It is customary to separate

the total heat transport into different components which are associated with different components of the velocity field such as the time mean flow or the eddy field (see e.g. Bryan 1982). The aim of course is to identify different physical mechanisms which have an effect on the mean heat transport and its possible variations in space and time.

2.1 The components of heat transport

For this purpose we consider the heat balance of the piece of ocean bounded to the south by the Antarctic continent (with coast line Γ_S) and to the north by a circumpolar belt (a surface Γ with circumpolar outcrops Γ_N at the sea surface and Γ_B at the bottom). Different shapes of the surface Γ will be specified later. The mass and heat balance of this piece of ocean may be expressed as

$$\begin{aligned} MF &= \int_\Gamma da\rho\omega = (MF)_{ICE} - \frac{\partial}{\partial t}MS \\ HF &= \int_\Gamma da\rho c_p T\omega = Q_{SURF} - L(MF)_{ICE} - \frac{\partial}{\partial t}HS \end{aligned} \tag{1}$$

where ω is the velocity component normal to Γ, $(MF)_{ICE}$ the mass flux of ice across Γ_S, L the latent heat of fusion of ice, da the area element on Γ, and Q_{SURF} the net heat flux across the ocean surface to the atmosphere (about $0.3PW$ if Γ_N is identified with the Polar Front). The storage terms for mass and heat are denoted by MS and HS, respectively. The density ρ and specific heat c_p will be treated as constant for the sake of simplicity.

The mass flux of icebergs $(MF)_{ICE}$ is in fact a fairly small contribution to any mass flux (and hence $L(MF)_{ICE}$ to any heat flux) considered in this problem. According to estimates of the mass balance of the Antarctic ice shield (e.g. Warrick and Oerlemans 1990) we find $(MF)_{ICE} \approx 10^{-7} kgs^{-1}$ corresponding to $10^{-4}Sv$ and hence $L(MF)_{ICE} \approx 10^{-3}PW$. We therefore neglect the ice flux across Γ_S. Furthermore, we split the circulation into its time mean (denote by an overbar) and deviation (denoted by a dash), i.e

$$q = \bar{q} + q' \tag{2}$$

for any quantity q. The part q' is identified with the transient eddies. The time mean mass and heat balance then is written in the simple form

$$\begin{aligned} \overline{MF} &= 0 \\ \overline{HF} &= \overline{Q}_{SURF}. \end{aligned} \tag{3}$$

Notice that the heat flux $\overline{HF}$ across the circumpolar belt Γ only depends on the shape of the surface outcrop Γ_N, all possible subsurface shapes must yield the identical normal heat transport equal to $\overline{Q}_{SURF}$. As a consequence of the vanishing of the net mass flux $\overline{MF}$ we further learn that $\overline{HF}$ is independent of the zero of the temperature scale, i.e.

$$\overline{HF} = \int_\Gamma da \rho c_p \overline{(T - T_0)\omega} \tag{4}$$

for any constant T_0. In fact this property enables us to identify $\overline{HF}$ as the flux of heat.

Our aim is now to identify the role of different physical mechanisms contributing to $\overline{HF}$ such as the heat transport by the time-mean flow and the transient eddies, by geostrophic and ageostrophic motions, by the barotropic and baroclinic flow or standing and transient eddies. It is quite obvious that any such separation must sum up to the same value $\overline{Q}_{SURF}$ for any given Γ_N. We will learn further that the importance of almost any of the mentioned components of the flow in carrying heat across Γ_N is highly dependent on the shape of Γ. In fact there is no sense in attributing specific magnitudes to any heat flux component in general.

The time mean heat flux may be expressed as sum of the heat flux HF^m due to the time mean flow and the contribution HF^e by the transient eddies

$$\overline{HF} = \int_\Gamma da \rho c_p \left(\bar{\omega}(\bar{T} - T_0) + \overline{\omega' T'}\right) = HF^m + HF^e. \tag{5}$$

Further separation concerns the time mean current $\bar{\omega}$. It may again be split into the geostrophic and ageostrophic parts

$$\bar{\omega} = \bar{\omega}_g + \bar{\omega}_{ag} \tag{6}$$

implying

$$\overline{HF} = HF_g^m + HF_{ag}^m + HF^e. \tag{7}$$

The ageostrophic motion is associated with the Ekman transport confined to the planetary boundary layers at the ocean surface and possibly frictionally controlled flow near the ocean bottom. Since vertical variations of the temperature are small in each of these boundary layers the heat flux by ageostrophic motion is fairly well approximated by

$$HF_{ag}^m = \oint_{\Gamma_N} ds \rho c_p (\bar{T}_{SURF} - T_0) V_{ag} \tag{8}$$

for the surface layer and correspondingly for the bottom part. Here

$$V_{ag} = \frac{\tau_s}{f} \tag{9}$$

is the local Ekman transport established by the wind component τ_s which is parallel to Γ_N. In contrast to $\overline{HF}$ or HF^m the Ekman contribution HF_{ag}^m is not independent of the temperature constant T_0 (since the net of V_{ag} does not vanish). We may thus obtain any desired value by suitably choosing T_0, e.g. $HF_{ag}^m = 0$ for a circumpolar path along $\bar{T}_{SURF} = T_0$.

A corresponding arbitrariness is attached to the geostrophic part

$$HF_g^m = \int_\Gamma da \rho c_p (\bar{T} - T_0) \bar{\omega}_g \tag{10}$$

by different choices of T_0 but also for different circumpolar belts Γ. Splitting $\bar{\omega}_g$ into the horizontal and vertical components we have

$$\begin{aligned} \bar{\mathbf{u}}_g &= (u_g, v_g) = \frac{1}{f} \hat{\nabla} \bar{p} \\ \bar{w}_g &= -\frac{\beta}{f} \int_z^0 dz' \bar{v}_g \end{aligned} \tag{11}$$

where u and v are zonal and meridional velocities, respectively, and $\hat{\mathbf{a}}$ is the vector resulting from couterclockwise rotation of $\mathbf{a}$ by $\pi/2$. We may rewrite (10) as

$$HF_g^m = \int_\Gamma da\rho c_p(\bar{T} - T_0)(\bar{\mathbf{u}}_g, \bar{w}_g) \cdot (\mathbf{n}_h, n_v) \tag{12}$$

where $(\mathbf{n}_h, n_v)$ is the unit vector which is locally perpendicular to Γ. The magnitude of the horizontal part is roughly estimated to be of order $1PW$ (with $\Delta T \sim 1K, \bar{v}_g \sim 0.01ms^{-1}$, ocean depth $h \sim 4000m$ and a circumpolar path of length $20000km$) while the contribution of the vertical part is usually much smaller (by a factor $\beta B/f \sim 0.05$ where B is the horizontal width covered by the belt Γ). However we easily find a belt for which the horizonal part vanishes identically and HF_g^m thus becomes very small of order $10^{-2}PW$. We may choose Γ as defined by the relation

$$\bar{p}(\mathbf{x}, z) - \bar{p}(\mathbf{x}_0, z) = 0 \tag{13}$$

for any point $\mathbf{x}_0$ on a circumpolar surface isobar. Then $\mathbf{n}_h \cdot \bar{\mathbf{u}}_g = 0$ and only the small vertical part of (12) remains,

$$HF_g^m = \int_\Gamma d^2x\rho c_p(\bar{T} - T_0)\bar{w}_g \tag{14}$$

Here $\bar{T}$ and $\bar{w}_g$ are evaluated on Γ but the integration extends over the horizontal projection of it. Notice that Γ is vertical at $\mathbf{x} = \mathbf{x}_0$ but is generally tilted at other locations. Obviously, transient eddies and frictional flow must carry the heat (at the required rate $\overline{Q}_{SURF}$) across the corresponding circumpolar path.

In quasigeostrophic scaling the above vertical contribution would not appear in the lowest (geostrophic) order of the theory. A further point to make in this context concerns the separation of the time mean fields into the zonal average and the deviation, called the standing eddy part (following atmospheric notation). Then the question of relative importance of the standing versus transient eddies in carrying heat across latitudes arises. However answers cannot be general if one extends the concept of standing eddies to other circumpolar paths. Obviously, there are no standing geostrophic eddies for the geostrophic streamline stack considered above.

Another peculiar belt was chosen by DeSzoeke and Levine (1981) in the only attempt (known to the author) made so far to estimate the heat flux

HF_g^m from oceanic observations. To circumvent the well-known problem of determining the absolute geostrophic current from hydrography they took Γ defined by the vertical belt of constant vertically integrated potential temperature

$$\Gamma : \int_{-h(\mathbf{x})}^{0} dz\bar{T}(\mathbf{x}, z) = T_1 = constant. \tag{15}$$

Separating the geostrophic velocity (which is now horizontal) into the barotropic and baroclinic components

$$\begin{aligned} \bar{u}_g &= \bar{u}_{bt}(s) + \bar{u}_{bc}(s, z) \\ \frac{\partial \bar{u}_{bc}}{\partial z} &= -\frac{g}{f}\frac{\partial \rho}{\partial s} \\ \int_{-h(\mathbf{x})}^{0} dz\bar{u}_{bc} &= 0 \end{aligned} \tag{16}$$

it is found that the unknown barotropic contribution cancels from the heat flux

$$\begin{aligned} HF_g^m &= \int_\Gamma da(\bar{u}_{bt} + \bar{u}_{bc})(\bar{T} - T_0) \\ &= \oint_\Gamma ds \int_{-h(\mathbf{x})}^{0} dz\bar{u}_{bc}(\bar{T} - T_0) \end{aligned} \tag{17}$$

if $T_0 = T_1$.

2.2 An estimate from hydrographic data

DeSzoeke and Levine (1981) applied this concept to a circumpolar path of constant vertically integrated potential temperature $T_1 = 1.3°C$ which is close to the Polar Front. It was found that the Ekman transport carries $28Sv$ and $0.15PW$ (with respect to $1.3°C$) across this path to the north. They further showed that the geostrophic heat transport is negligibly small, $HF_g^m \simeq 0$ with a minimum error of $0.05PW$ (assuming that data at different levels are totally uncorrelated) and a worst error of $0.23PW$ (assuming perfect correlation which is highly unlikely). The heat balance then reads

$$\begin{array}{rcl} HF_g^m + HF_{ag}^m + HF^e + HF_{miss} = & \overline{Q}_{SURF} \\ 0 \quad + \; 0.15 \; + \quad ? \quad + \quad ? & = -0.30PW \end{array}$$

where HF_{miss} stands for possibly overlooked contributions, perhaps associated with frictional flow near the bottom, inertial flows in deep canyons or unresolved geostrophic motion. This latter problem may particularly concern Antarctic Bottom Water ($AABW$) escaping the course station spacing close to the bottom. The transport of the cold $AABW$ is not well known, values between 2 and $25Sv$ are given by various authors (see e.g. Fahrbach et al. 1992). The lower range of these values applies to more southerly latitudes close to the formation regions around Antarctica. Further north the definition of $AABW$ is widened to include waters entrained by mixing processes. We will discuss one of the most important formation processes of $AABW$ in chapter 4 in more detail and suggest that $10Sv$ is a realistic upper bound for the formation rate all around Antarctica. With a volume transport of $10Sv$, at $-0.5°C$, the $AABW$ would transport $0.07PW$ (with respect to $1.3°C$) to the south.

The above balance thus requires a substantial contribution from the turbulent eddy field which is known from satellite altimetry and other in-situ observations to be particularly vigorous in this part of the world ocean. To close the heat balance of the Southern Ocean south of the Polar Front the eddies must carry about $0.4PW$ to the south (the uncertainty of this estimate is quite large, possibly $\pm 0.2PW$). Bryden (1983) has estimated the heat of an individual eddy in the Drake Passage area as $0.013PW$ so that about 20 to 30 eddies of this size are required at any time around the circumpolar belt to accomplish the $0.4PW$. This appears to be a reasonable number. Nowlin and Klinck (1986) support this magnitude of the heat flux due to single eddies by other observations.

We can also support this magnitude by results from consideration of the momentum balance of the ACC. We will show below in chapter 3 that lateral transport of heat and the vertical transfer of momentum through the water column are mutually dependent. It is for this reason that the momentum balance of the flow along the Polar Front has strong implications for the heat transport across it.

3 The circumpolar link: the strength of the Antarctic Circumpolar Current

The wind-driven branch of the circulation in the world ocean is structured in cells which are approximately confined to separate ocean basins. In

the thermohaline branch the basins are however connected. The deep ventilation is triggered by production of cold dense water masses in high latitudes of the North Atlantic and the Southern Ocean and penetrate from there into the other basins. The deep water formed in the North Atlantic moves south across the equator into the circumpolar region and is carried by the *ACC* into the Indian and Pacific Oceans. It spreads in these basins even further north with gradual upwelling all along its path and concentrated upwelling in the equatorial regions. The loop is closed by the current system in the surface layers and transport (of salinity and passive tracers) induced by transient motions, forming a huge conveyor belt (e.g. Gordon 1986) which connects all basins of the world ocean. The water masses formed in the Southern Ocean (see chapter 4) spread with and across the *ACC* and fill the bottom layer of all ocean basins (e.g. Emery and Meincke 1986).

The *ACC* is thus a major conduit in the thermohaline ventilation system. Its strength is set by the reaction of the fluid to the forcing functions – wind and buoyancy flux at the surface – and the geometry and topography of the circumpolar domain. Measuring the transport and internal structure of the current and understanding its dynamical balance has long been a major task of research (see e.g. the review of Nowlin and Klinck 1986). The strong eastward surface wind stress in the circumpolar belt must obviously be considered as principle driving agent. The problem of early concepts of the balance was to find an effective sink of momentum. In the latitude band of the Drake Passage there are no continental barriers which could support a net zonal pressure gradient as in the other basins and thereby oppose the acceleration of the current by the wind. Conventional parametrisation of friction – in the form of lateral or vertical diffusion of momentum or bottom friction – gave rather unsatisfactory results (Hidaka and Tsuchiya 1953, Gill 1968 and others). The current amplitudes in these models are proportional to the applied wind stress and inversely proportional to the values of the frictional parameters, e.g. for lateral friction the mass transport scales as $\tau_s D^3/A_h$ where τ_s is the wind stress amplitude, D the current width and A_h the lateral eddy viscosity. Hidaka thus faced the difficulty of explaining the observed transport values of about $100Sv$ with reasonable values for the model friction and the observed wind stress.

In one of the earliest papers on this problem Munk and Palmén (1951) suggested a solution which today still appears as the only acceptable way out of a frictionally controlled balance of the current. Though continental barriers are absent, there are significant submarine ridges to build up net zonal pressure gradients. Munk and Palmén speculate that this could enable a transfer of momentum to the solid earth. A balance with the

wind stress can occur only if the flow establishes pressure differences across the ridges with the appropriate sign (higher pressure value on the western side for westerly winds) and magnitude. To balance a stress of $10^{-4}m^2s^{-2}$ a pressure difference of only a few dynamic centimeters is required across a ridge of a few thousand kilometers.

For this balance to operate, the momentum given to the ocean at the surface must be transferred down to the blocked depths where the flux by pressure differences across topography into the solid earth - the so-called topographic form stress or mountain drag - can be effective. This vertical transport of momentum must be extremely large compared to other oceanic areas. To transmit the wind stress of the above magnitude in the observed vertical current shear of about $0.1ms^{-1}$ over 1000m by vertical diffusion, an equivalent value of vertical eddy viscosity of $1m^2s^{-1}$ is needed. This is three or even four orders of magnitude larger than elsewhere (large scale oceanic models generally use $10^{-4}m^2s^{-1}$). However, inverse models of the ACC which are based on hydrographic data, fully support these high values of the vertical transport of momentum (Olbers and Wenzel 1989).

Three-dimensional turbulence of small scale is unlikely to support such a large transport of momentum. However, turbulence of larger scale – meso-scale quasigeostrophic eddies – populate the current. Generated by mixed barotropic-baroclinic instability of the mean flow the mesoscale eddies are crucial to achieve the balance of the current.

3.1 The role of eddies in the dynamical balance

Like other large-scale ocean currents the *ACC* is in geostrophic balance: the horizontal velocity component in the direction of the flow is – to a very good approximation – given by the pressure gradient across it. However, this relation does not give insight into the dynamical balance of the flow, asking for the principle external forces imparting momentum into the fluid, the mechanisms which redistribute it in the interior, and the sinks by which the momentum leaves the fluid, ultimately allowing for a steady state (possibly after averaging over the time scale of transient eddies) and determining the strength of the current. The answer to this question resides in projections of the momentum balance equations which are not dominated by the geostrophic relation, as e.g. the component of the balance along the flow.

Introducing horizontal coordinates s along an arbitrary circumpolar path on the depth level z and n normal to it the s-component of the momentum balance reads

$$[\frac{\partial \bar{u}}{\partial t}] - (f + \bar{\zeta})\bar{v} + \bar{w}\bar{\eta} = -\frac{\partial}{\partial s}\left(\bar{p} + \frac{1}{2}(\bar{u}^2 + \bar{v}^2 + \bar{w}^2)\right) + \mathcal{F} + \mathcal{E} \qquad (18)$$

where (u, v, w) is the velocity vector in (s, n, z)-coordinates and η and ζ are the n- and z-components of the relative vorticity, respectively. $\mathcal{F}$ denotes frictional terms and $\mathcal{E}$ the terms arising from transient eddies. The vanishing time rate of change is included here for easier identification. As mentioned above, $\bar{u}$ is in approximate geostrophic balance

$$f\bar{u} = -\frac{\partial \bar{p}}{\partial n} \qquad (19)$$

and $\bar{v} = 0$ if the path is oriented along the streamline of the time mean flow (s, n then define the natural coordinates of the mean flow).

The external forcing by wind stress couples to the friction term $\mathcal{F}$ if (18) is integrated vertically from the surface to any depth. Thermohaline forcing, however, enters only indirectly via its effect on the baroclinic part of the pressure field.

The geostrophic terms almost entirely cancel by averaging (18) around the circumpolar path,

$$\oint ds\,(-(f + \bar{\zeta})\bar{v} + \bar{w}\bar{\eta}) = \oint ds(\mathcal{E} + \mathcal{F}) - \sum_{ridges} \Delta(\bar{p} + \frac{1}{2}\bar{v}^2). \qquad (20)$$

The only pressure forces remaining are those acting on submarine ridges which intersect the path at the level z.

Terms involving vertical advection (time mean and eddies) are small, in quasigeostrophic (QG) scaling they do not appear in the lowest order approximation of (18). Furthermore, since the circumpolar average of the geostrophic velocity vanishes, the Coriolis term is dominated by the ageostrophic velocity. Abbreviating the circumpolar integration by cornered brackets we have

$$< f\bar{v} > \approx f_0 < \bar{v}_{ag} > + \sum_{ridges} \Delta\bar{p}_g \qquad (21)$$

and in QG scaling (20) then reads

$$-f_0 < \bar{v}_{ag} > - < \bar{v}_g \bar{\zeta}_g > = < \mathcal{F} > + < \mathcal{E} > - \sum_{ridges} \Delta(\bar{p}_{ag} + \frac{1}{2}\bar{v}_g^2). \quad (22)$$

Considering a geostrophic streamline as a circumpolar contour (so that $\bar{v}_g$ vanishes) it becomes clear at this stage that eddy and frictional effects must be important at levels where the path is not interrupted by topography. Below such levels the pressure force on submarine mountains may come into play. We will substantiate the importance of these terms below.

In the circumpolar average the term $\mathcal{E}$ representing the direct effect of transient eddies becomes

$$< \mathcal{E} > = < \overline{v'\zeta'} > - \sum_{ridges} \Delta(\frac{1}{2}\overline{v'^2}). \quad (23)$$

There are however indirect effects of transient eddies buried in the ageostrophic Coriolis force. Integrating the mass conservation equation over the horizontal area enclosed by the circumpolar path and the coastline of Antarctica and utilizing the buoyancy balance in the adiabatic form, it is found that the ageostrophic flow across the path is related to the lateral (mean and eddy) flux of buoyancy in the form

$$f_0 < \bar{v}_{ag} > = \frac{\partial}{\partial z} \frac{f_0}{N^2} < \bar{v}_g \bar{b} + \overline{v'b'} > \quad (24)$$

where b is the buoyancy and N the Brunt-Väisälä frequency. The averaged momentum balance (22) may then conveniently be rewritten in terms of the lateral (mean and eddy) flux of the QG potential vorticity

$$Q = f + \zeta_g + \frac{\partial}{\partial z} \frac{f_0}{N^2} b. \quad (25)$$

The flux due to transient eddies is given by

$$< \overline{v'Q'} > = < \overline{v'\zeta'} > + \frac{\partial}{\partial z} \frac{f_0}{N^2} < \overline{v'b'} > \quad (26)$$

The thermal wind relation allows to commute v with the vertical derivative. A corresponding expression holds for $< \bar{v}_g \bar{Q} >$. The balance (22) then becomes

$$-(< \bar{v}_g \bar{Q} > + < \overline{v'Q'} >) =< \mathcal{F} > - \sum_{ridges} \Delta \left(\bar{p}_{ag} + \frac{1}{2}(\bar{v}_g^2 + \overline{v'^2}) \right) . \quad (27)$$

This equation expresses the dynamical balance of the *ACC* as the interplay of three distinct physical processes: those arising from eddies, friction and the time-mean pressure field. The frictional force $\mathcal{F}$ stems from the transfer of momentum due to mechanically driven three-dimensional small scale turbulence limited to the near-surface layer which is directly stirred by the wind. The terms on the lhs represent the lateral fluxes of potential vorticity. Notice that the first term describes the flux due to stationary standing eddies (evaluated with respect to the given arbitrary circumpolar contour). The second term is the flux of potential vorticity due to the transient eddies in the current. This flux is thus achieved by meso-scale turbulent motion which is quasi-two-dimensional and geostrophically balanced.

The eddy flux of potential vorticity consists of two parts. The lateral eddy relative vorticity flux $< \overline{v'\zeta'} >$ represents the convergence of eddy momentum fluxes. We show below that this is just the familiar (negative) meridional divergence of the Reynolds stress $< \overline{u'v'} >$ if the path is oriented zonally. The physics of the second part may be more easily understood if the buoyancy b' is replaced by the vertical displacement $z' = -b'/N^2$ of the mean isopycnals by the eddies. The eddy buoyancy flux

$$< \overline{v'b'} >= -N^2 < \overline{v'z'} >= -\frac{N^2}{f_0} < z' \overline{\frac{\partial p'}{\partial s}} >= \frac{N^2}{f_0} < p' \overline{\frac{\partial z'}{\partial s}} > \quad (28)$$

is then related to the eddy interfacial form stress $< \overline{z' \partial p'/\partial s} >$. It describes the acceleration of fluid by horizontal pressure forces $\partial p/\partial s$ on the eddy scale across the tilted interface $z' = const$ of a material fluid volume thus establishing a vertical transport of horizontal momentum (see e.g Rhines and Holland (1977) or Johnson and Bryden (1989)). In this Lagrangian framework the eddy buoyancy flux represents a vertical transfer of momentum through the water column. A similar reasoning applies to the contribution due to standing eddies.

The third process – the pressure forces on submarine mountains – acts only when the circumpolar contour hits submarine ridges. In the *ACC* belt this occurs at levels below about $2000m$ depth. This pressure force is a property of the time mean flow; it results by adjustment of the mass field to wind and thermohaline forcing and to the geometry and topography of the ocean basin (see e.g. Olbers et al. 1993).

The momentum balance for any layer of fluid is obtained by vertical integration. If the layer extends from a level $z = z_0$ to the bottom $z = -h(s)$ on the contour, the ageostrophic pressure force converts to a stress

$$\int_{-h_{max}}^{z_0} dz \sum_{ridges} \Delta \bar{p}_{ag} = - < \bar{p}_{ag} \frac{\partial h}{\partial s} > = < h \frac{\partial \bar{p}_{ag}}{\partial s} > \tag{29}$$

The corresponding geostrophic part of this stress results from the integration of the stretching term of the potential vorticity flux of the standing eddies

$$\int_{-h_{max}}^{z_0} dz < \bar{v}_g \bar{Q} > = \int_{-h_{max}}^{z_0} dz < \bar{v}_g \bar{\zeta}_g > - < h \frac{\partial \bar{p}_g}{\partial s} > \tag{30}$$

The stress $< h \partial \bar{p} / \partial s >$ is known as the bottom form stress or mountain drag. It transfers momentum from the fluid to the earth (or vice versa, in this case it is not a drag) by the time mean horizontal pressure force at the bottom. Apparently, this can work only if the ocean depth and the bottom pressure are out of phase. To lowest order in geostrophic scaling the bottom form stress may be evaluated using the geostrophic pressure field at the bottom.

The standing eddy contribution vanishes identically if the contour is a geostrophic streamline. In this case the flux of potential vorticity due to transient eddies remains to balance the frictional stress divergence and the pressure force. We see again – as discussed above for the heat flux – that the importance of contour-averaged flux terms depends very much on the shape of the contour. At levels which are not constrained by topography we then get the dynamical balance in the simple form

$$- < \overline{v' Q'} > = < \mathcal{F} > = \frac{\partial < \bar{\tau} >}{\partial z} \tag{31}$$

where τ is the frictional stress component parallel to the contour at level z (lateral friction may be neglected if eddies are resolved). Below the wind-mixed layer where the frictional stress vanishes the lateral flux of potential vorticity must vanish identically. This does not mean that eddies are absent or have no effect on the mean flow, rather it is indicating that different contributions to the eddy flux $< \overline{v'Q'} >$ compensate. As we know from chapter 2 the eddies must be quite vigorous to carry heat across circumpolar latitudes. The connection to the flux of potential vorticity is drawn below in section 3.3. We should realize here that the vanishing of $< \overline{v'Q'} >$ in the ocean interior requires the absence of a large-scale gradient of potential vorticity. Overwelming evidence of nearly constant potential vorticity on isopycnals in the Southern Ocean has been presented by Marshall et al. (1993).

Equation (27) gives a convenient framework to analyse the dynamical balance of a circumpolar flow. In the traditional view, s is taken along the zonal direction. Alternatively, natural coordinates may be taken, in which case s is along the streamline of the time mean geostrophic flow (e.g. Marshall et al. 1993). This approach highlights the underlying physics and role of the transient eddies, since standing eddies are absent. The relation between the normal eddy flux across an arbitrary path - established by standing and transient components - and the flux across a mean streamline - established by transients alone - is readily obtained by integrating the time-average potential vorticity balance over the enclosed area, resulting in

$$\oint_{any\ path} ds(\bar{v}_g\bar{Q} + \overline{v'Q'}) - \oint_{streamline} \overline{v'Q'} = \\ = \int_{enclosed\ area} dA\, \mathbf{k} \cdot \nabla \times \frac{\partial \tau}{\partial z}. \tag{32}$$

If there is no applied stress or friction – as in the interior where $\tau = 0$ – we see that the sum of steady and transient eddies across any contour is exactly equal to the transient eddy flux across a mean streamline. This points out the eminent role of the transient motions in the dynamical balance.

Other forms of the potential vorticity flux may be more familiar to the reader. Considering for example a zonal contour and for simplicity quasi-Cartesian coordinates we find

$$< \overline{v'Q'} > - \sum_{ridges} \frac{1}{2} < \overline{v'^2} >= -\frac{\partial}{\partial y} < \overline{u'v'} > + \frac{\partial}{\partial z} < \overline{p' \frac{\partial z'}{\partial x}} > \qquad (33)$$

$$= (\frac{\partial}{\partial y}, \frac{\partial}{\partial z}) \cdot (- < \overline{u'v'} >, < \overline{p' \frac{\partial z'}{\partial x}} >). \qquad (34)$$

As outlined above the first term in (33) describes the horizontal convergence of momentum, it arises directly from eddy terms in the momentum balance. The second term decribes vertical convergence of momentum and arises from the mean ageostrophic Coriolis force. The second identity (34) involves the divergence of the Eliassen-Palm vector, here written for the transient eddies (Eliassen and Palm 1961, see also Stevens and Ivchenko (1993) for the context of the *ACC*).

We should emphasize that the balances have been derived in this chapter on the basis of quasigeostrophic dynamics. Their essential form still applies to more complete physics. If we abandon the *QG* scaling the terms associated with vertical advection (mean and eddy) of momentum and buoyancy reappear in the balance (27), in particular the vertical eddy-induced flux $< \overline{u'w'} >$ of momentum. These terms are small. Including the thermodynamics considered in primitive equation models, however, adds another term in (27). In particular south of the *ACC* diabatic sources of buoyancy must be considered which force ageostrophic flow across the circumpolar path. A source S (the divergence of a flux of buoyancy due to convection or diffusion) in the buoyancy balance at any vertical level z converts to an integral over the area enclosed by the coastline and the circumpolar path in the form

$$f_0 V_0(z) = \frac{\partial}{\partial z} \int dA \frac{gS}{N^2} \qquad (35)$$

in (24) and appears in addition to the standing and transient eddy flux divergences of buoyancy in the dynamical balance (27) which then takes the more general form

$$\begin{aligned} -(< \bar{v}_g \bar{Q} > + < \overline{v'Q'} >) = \\ = f_0 V_0(z) + < \mathcal{F} > - \sum_{ridges} \Delta \left(\bar{p}_{ag} + \frac{1}{2}(\bar{v}_g^2 + \overline{v'^2}) \right). \end{aligned} \qquad (36)$$

Notice that the diabatic buoyancy sources stand on equal footing with the viscous terms, i.e. they appear in the form of vertical fluxes.

3.2 The dynamical balance in eddy resolving models of the Southern Ocean

It has only recently become possible to run full primitive equation models with eddy resolution in large ocean domains. The Southern Ocean presents a particular problem because of its vast area and its weak stratification (the baroclinic Rossby radius is between $5km$ and $15km$ (Houry et al. 1987)). If full thermodynamics are included and the stratification is realistic as e.g. in the Fine Resolution Antarctic Model (FRAM), eddies tend to be only marginally resolved (see FRAM 1991). On the other hand QG models of the ACC can choose the Rossby radii in relation to the given resolution of the model. These models therefore generally run with eddy resolution but too strong stratification.

The dynamical balance of a zonally-periodic current has been investigated in many eddy resolving multilayer channel models with QG dynamics and idealised topography (e.g. McWilliams et al. 1978, Wolff and Olbers 1989, Treguier and McWilliams 1990, Wolff et al. 1991, Marshall et al. 1993). These investigations have promoted the scenario first proposed by Munk and Palmén (1951): the momentum imparted by the wind to the fluid at the surface is carried down through the water column by the eddies and leaves the fluid via bottom form drag (this mechanism deccelerates the earth). These processes have been discussed above. Below the surface layer the momentum balance is thus essentially frictionless. Recent analysis of a QG model of the Southern Ocean with realistic geometry and topography (Wolf-Gladrow et al. 1993) and the $FRAM$ model (Stevens and Ivchenko 1993) only marginally altered the basic concept. The latter authors showed in particular that the ageostrophic flow induced by diabatic physics cannot be neglected, i.e. the term $f_0 V_0$ is not small in (36).

The realistic QG model of the ACC is an extension of the classical β–plane channels used as an idealization of the circumpolar flow around the Antarctic continent. It has three layers of depth $1000m, 1500m$ and $2500m$ and a horizontal resolution of $1/3°$ zonally and $1/6°$ meridionally which the resolves the wave scale of the Rossby radius quite well (the baroclinic Rossby radii are $18km$ and $9km$). The domain extends from $40°S$ to the Antarctic continent. The coast line is the $500m$ depth contour around the continents, while at $40°S$ the model domain is closed by a solid wall. The deep ocean topography is a linear unsmoothed interpolation

the 12′–data of the *DBDB5* data (Heirtzler 1985) on the model grid. The topographic height above $5000m$ is then scaled down to 20% following quasi-geostrophic requirements.

An instantaneous view of the circulation in the upper layer is shown in Figure 1. It exhibits the *ACC* (visible as the thin continuous bands associated with the fronts) imbedded in an intense mesoscale eddy variability. The latter is mostly found in areas with strong topographic features - namely the area behind the Drake Passage, the Kerguelen in the sector of the Indian Ocean and the Maquarie Ridge area south of New Zealand. The flow has a strong barotropic component so that the currents at deeper levels appear rather similar.

Figure 2 displays the terms of the zonally averaged balance of the zonal momentum of the three layers of the model. The dynamical balance (27) is thus considered with averaging along latitudes and integration is performed over the individual layers. The vertical divergence of the interfacial form stress then appears as the difference between the values at the top and bottom of each layer and the pressure force on the bottom converts to the bottom form stress as given by (29) and (30). Zonal averaging has also been applied to latitudes that are blocked by continents (South America north of $55°S$ and the Antarctic Peninsula south of $62°S$) so that in addition to the terms considered for unconstrained latitudes, a pressure force appears in the balance by which the flow acts on the continental barriers. In contrast to the bottom form stress which to lowest non-vanishing order can be evaluated geostrophically, this pressure force on continents contains the ageostrophic pressure (the geostrophic pressure cancels since the continental boundary is a geostrophic streamline). It is shown in Wolf-Gladrow et al. (1993) how the ageostrophic pressure is calculated on solid lateral boundaries.

It is seen in the figures that the wind input in the top layer is compensated almost entirely by the eddy interfacial form stress. This mechanism hands the momentum down through the water column to the bottom layer. Here it leaves via the bottom form stress. All explicit friction terms are negligible, also the horizontal Reynolds stresses caused by the eddies and the pressure force on continents have only a minor role. They are not shown on the figures.

The terms of the balance are combined in Figure 3 to the lateral flux of potential vorticity by the eddies (transient and standing) as described in the preceding chapter. Apparently, in the middle layer, which has no explicit friction, the eddy flux of potential vorticity is fairly small. This is also valid in the bottom layer since bottom friction is small. In the top layer, however, the eddy flux is balanced by the prescribed wind stress. It should be noted that in the interior where vorticity sources are

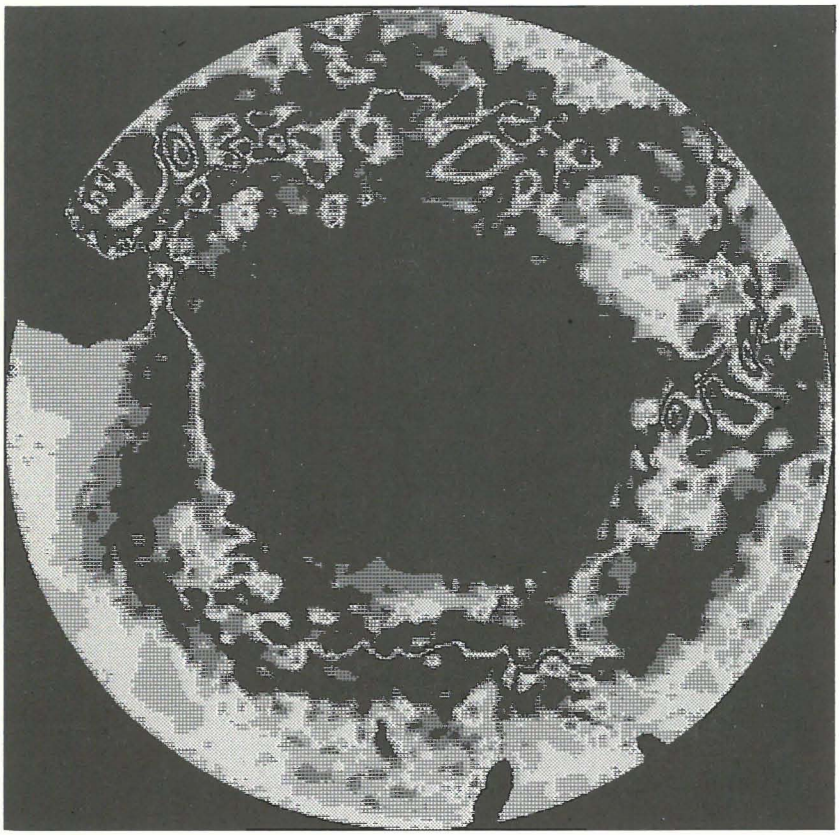

Figure 1: An instananeous view of the streamfunction in the top layer of the quasigeostrophic simulation of the *ACC*. The streamfunction is displayed in gray shading (the scale is repeated three times, each step corresponds to approximately $2Sv$. The transport in this layer is $74Sv$, the two deeper layers carry $105Sv$.

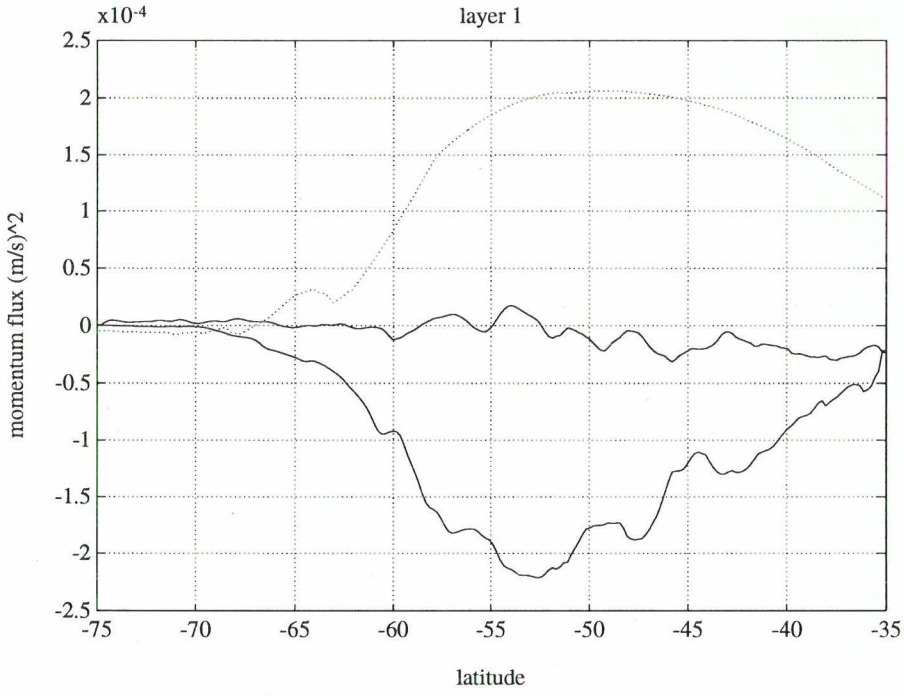
x10-4
layer 1
momentum flux (m/s)^2
2.5
2
1.5
1
0.5
0
-0.5
-1
-1.5
-2
-2.5
-75
-70
-65
-60
-55
-50
-45
-40
-35
latitude

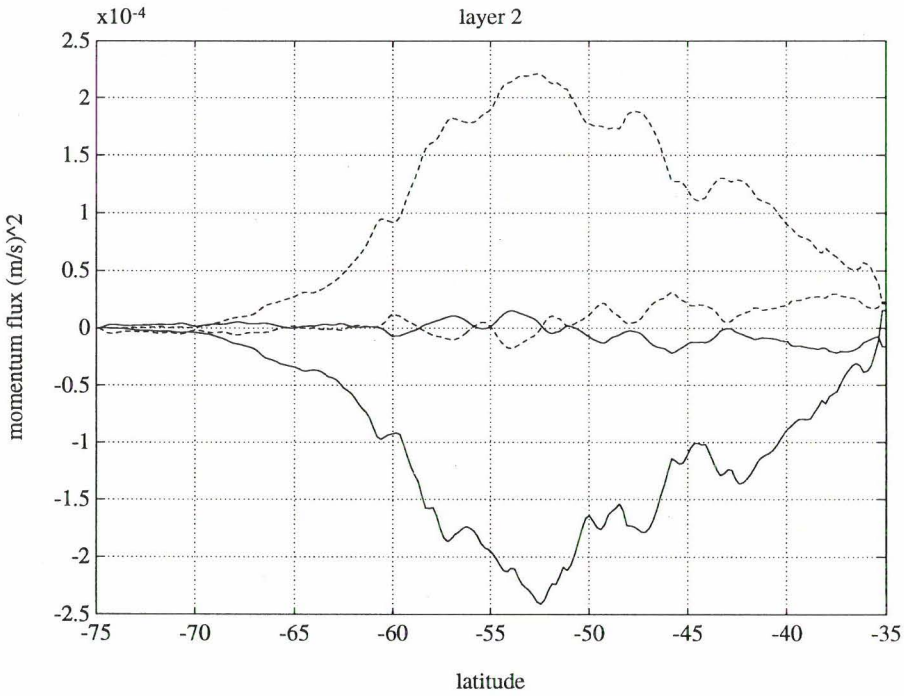
x10-4
layer 2
momentum flux (m/s)^2
2.5
2
1.5
1
0.5
0
-0.5
-1
-1.5
-2
-2.5
-75
-70
-65
-60
-55
-50
-45
-40
-35
latitude

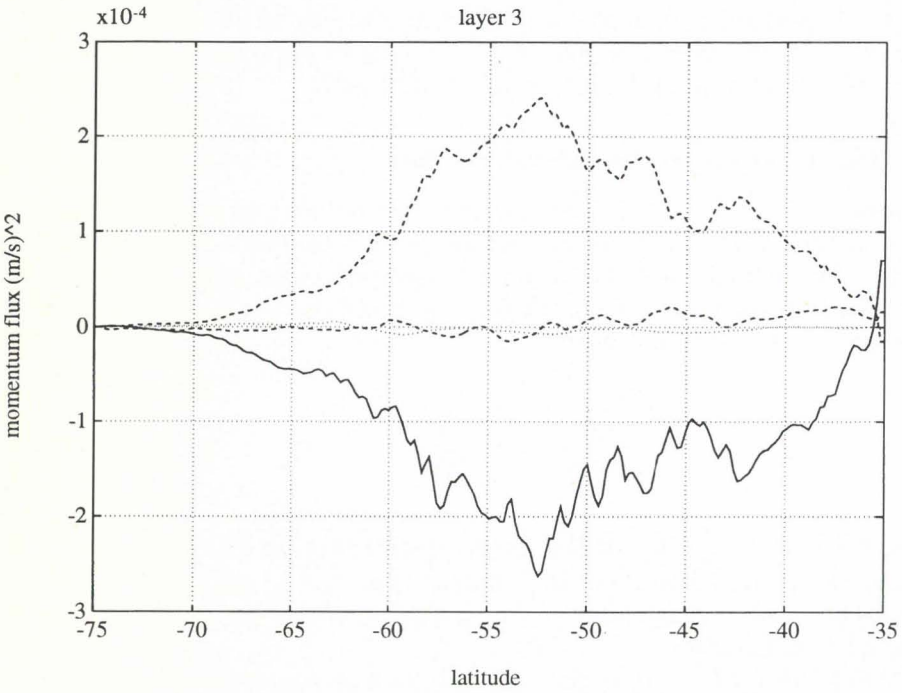

Figure 2: The time and zonally averaged zonal momentum balance for the three layers of the quasigeostrophic simulation of the *ACC*. The three panels display the wind input (in the top layer 1), the bottom friction and the bottom form stress (in the bottom layer 3), and the standing and transient interfacial form stresses (in all three layers). The frictional fluxes are plotted in dotted lines, the form stresses in dashed lines if they are sources of momentum for the particular layer, or solid lines if they are sinks of momentum. In each case the transient eddies term is the smaller contribution.

absent, the potential vorticity becomes homogeneous as a consequence of the mixing by the vigorous eddy field. This is in good agreement with observation of this quantity (Marshall et al. 1993).

3.3 The relation to the eddy heat flux

The momentum balance of the mean flow can be used to infer the magnitude of the meridional heat flux across the *ACC* (i.e. the Polar Front). The interfacial eddy form stress can be expressed in terms of the lateral eddy heat transport by relating the buoyancy and temperature variations of the eddies (neglecting salinity)

$$\frac{<\overline{v'b'}>}{N^2} = \frac{<\overline{v'T'}>}{\frac{dT_m}{dz}} \tag{37}$$

where $T_m(z)$ is the profile of the mean stratification in the area. A corresponding relation holds for the contribution due to standing eddies. We can however concentrate on the transient eddies by considering a geostrophic streamline.

We have seen above that the redistribution of momentum by lateral Reynolds stresses is small. Below the wind-driven layer, frictional effects are small so that by (26) and (31) the eddy heat flux in the water column is a constant. Its magnitude is set by the surface wind stress τ_s (Marshall et al. 1993). Integration of (31) yields for these conditions

$$[<\overline{v'T'}>)]_{z=0}^{z} = \frac{\tau_s}{f_0}\frac{dT_m}{dz}. \tag{38}$$

This implies that the eddy-driven northward heat flux is given approximately by

$$HF^e = hL\rho c_p \frac{\tau_s}{f_0}\frac{dT_m}{dz} \tag{39}$$

where h is the ocean depth and L is the circumference of the path in question. The total meridional heat flux by the eddies in the circumpolar belt is thus set via the dynamical balance of the *ACC* by the surface wind stress. With reasonable numbers for the stratification at the Polar Front ($dT_m/dz \sim 3°C/4000m, \tau_s \sim 10^{-4}m^2s^{-2}$) we find an eddy heat flux

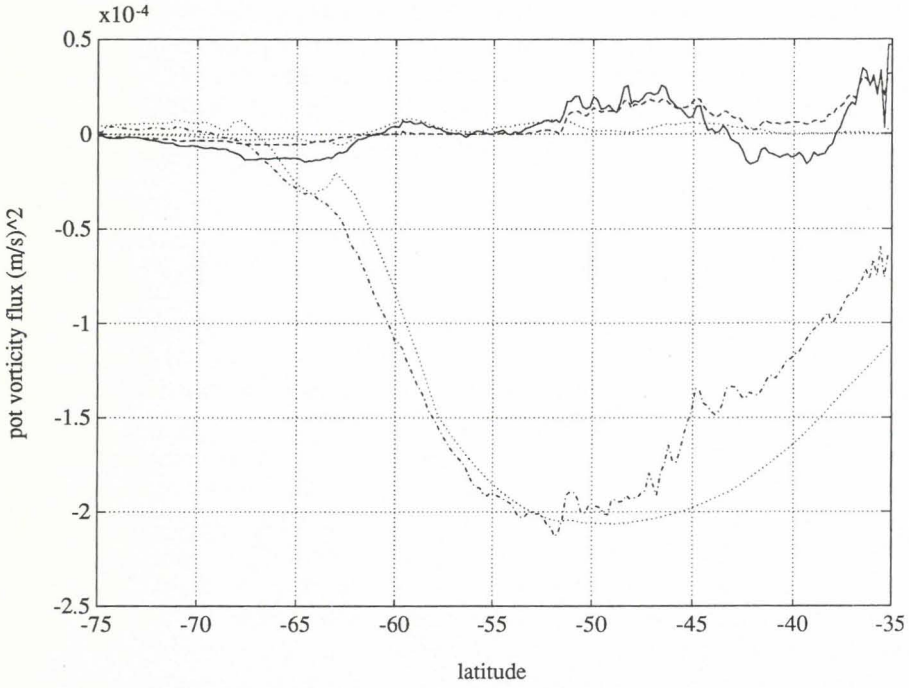

Figure 3: The time and zonally averaged potential vorticity flux (the sum of standing and transient eddies) and the friction terms for the three layers of the QG model. The friction terms are dotted lines, potential vorticity flux in the top layer is dashdot, the flux in the intermediate layer is the dashed line, and the flux in the bottom layer is the solid line.

of magnitude $0.24PW$ to the south as required by the rough analysis given in chapter 2. Though this result has been supported here by a model based on reduced physics it should also apply in a full ocean eddy resolving model and in the real ocean. It emerges out of the generally accepted scenario of a dynamical balance for the *ACC*.

4 The water mass connection: formation of Antarctic Bottom Water

Oceanic motions are approximately adiabatic. Once a water parcel has got its imprint of temperature and salinity by heat and freshwater exchange with the air at the sea surface it conserves potential temperature and salinity thus moving on isopycnals. The distribution of potential density in the world ocean – as exemplified by the zonally averaged meridional distribution (Figure 4) – shows that the deep cold water masses must originate from the polar seas. There is a drastic mismatch between the volume of the cold water sphere and its window at the sea surface through which the density structure allows interaction with the atmosphere. As an example, water with temperatures below $4°C$ occupy 75% of the ocean volume but are in contact with atmosphere at only 4% of the sea surface. These polar gateways of the cold water sphere are thought to define the key role of the polar oceans in global climate.

Formation of deep water takes place in northern and southern high latitudes but the deepest and coldest water of the world ocean originates entirely in the south. Antarctic Bottom Water (*AABW*) spreads far into the northern hemisphere filling the deep layers and influencing directly about 30% of the ocean volume (Worthington 1981).

AABW is produced by a range of delicate formation processes which involve deep reaching convection within cells of very small diameter, and intricate mixing processes of water masses modified by sea ice freezing and shelf ice melting on the continental shelf and slope. The formation occurs south of the Polar Front either in the open ocean or along the continental margin, the latter predominantly in the southern Weddell Sea where according to Carmack (1977) 70% of the total *AABW* is formed. The basic mechanisms of the formation are understood (see e.g. Carmack 1986). Only little, however, is known of the interplay of all the ingredients of *AABW* production and transport - convection, mixing and propagation - in particular the rates of formation and transport are subject to wild speculations. We can be sure that all these processes are not adequately included in any of the coarse ocean circulation models used for climate studies.

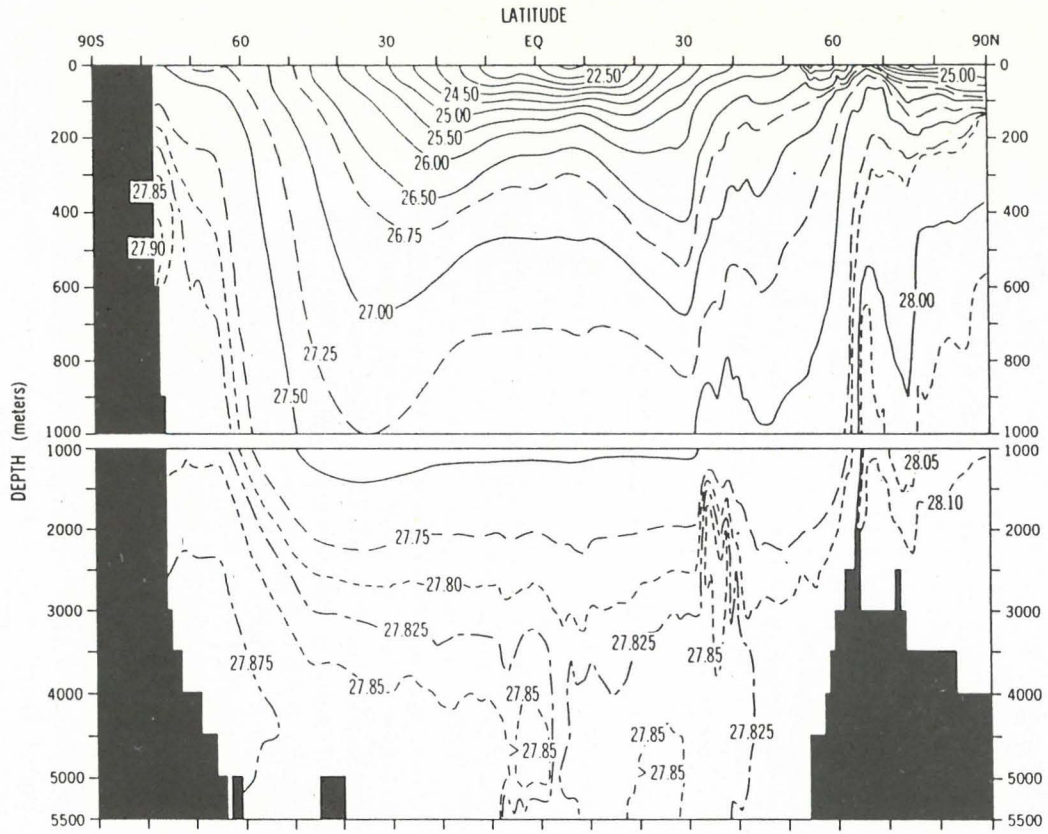

Figure 4: A section of the zonally averaged potential density in the world ocean (units $10^{-3} gcm^{-3}$), (from Levitus 1982).

The ultimate product *AABW* - in various different characteristic temperature/salinity combinations as a consequence of the different formation processes and regions - is assumed to leave the Southern Ocean via deep boundary currents along topographic barriers into the northern ocean basins. Any change in the environmental conditions leading to the production and transport of *AABW* will have an effect on the meridional heat transport. The *AABW* component of the heat flux across the Polar Front was estimated above to be roughly $0.07PW$ to the south. It was based on a transport of $10Sv$ across the Polar Front. We will demonstrate the range of uncertainty of this value by modelling the dominant formation process in the Weddell Sea.

4.1 Formation of *AABW* in the Weddell Sea

The interior of this subpolar gyre is filled with three water masses sitting on top of each other: the Warm Deep Water (*WDW*, roughly 30% of volume, below the surface water masses down to roughly $1000m$ depth) with temperatures in the range $0°C$ to $0.8°C$, a broad layer of *AABW* (about 57%, between $1000m$ and $4500m$ depth) in the range $-0.8°C$ to $0°C$ and a thin layer of cold Weddell Sea Bottom Water (*WSBW*, roughly 3%) in the range $-1.4°C$ to $-0.8°C$. Figure 5 shows these water masses for a section across the Weddell Gyre made during the Winter Weddell Gyre Study in October 1989 (Fahrbach et al. 1991).

Traditionally *AABW* is considered as the mixing product of *WDW* and *WSBW* (see the *T-S*-diagrams in Figure 6). Following the hypothesis of Foster and Carmack (1976) *WSBW* is formed on the continental shelf in a series of mixing processes involving *WDW* and two further species: Western Shelf Water (*WSW*) - resulting from sea ice freezing on the shelf - and Winter Water (*WW*) which is a remnant of sea ice formation outside the shelf in the open ocean. Foldvig et al. (1985a) suggested an alternative route to *AABW*: according to their hypothesis *WSBW* results from mixing of *WDW* and Ice Shelf Water (*ISW*). This latter is a very cold species (-2.4 to $-2.0°C$) which is formed by thermohaline processes under the huge Filchner and Ronne Ice Shelves flowing from the Antarctic continent out on top of the ocean. Potential temperature sections parallel to the ice shelf edges, representing typical Antarctic summer conditions, reveal distinct cores of *ISW* with temperatures as low as $-2.2°C$ which is well below the freezing point at the surface (about $-1.87°C$ at salinity 35.0).

Sverdrup (1940) assumed that *ISW* results from the modification of shelf water masses due to heat loss at the base of deep-drafting ice shelves. A more detailed description concerning the whole sub-ice shelf system

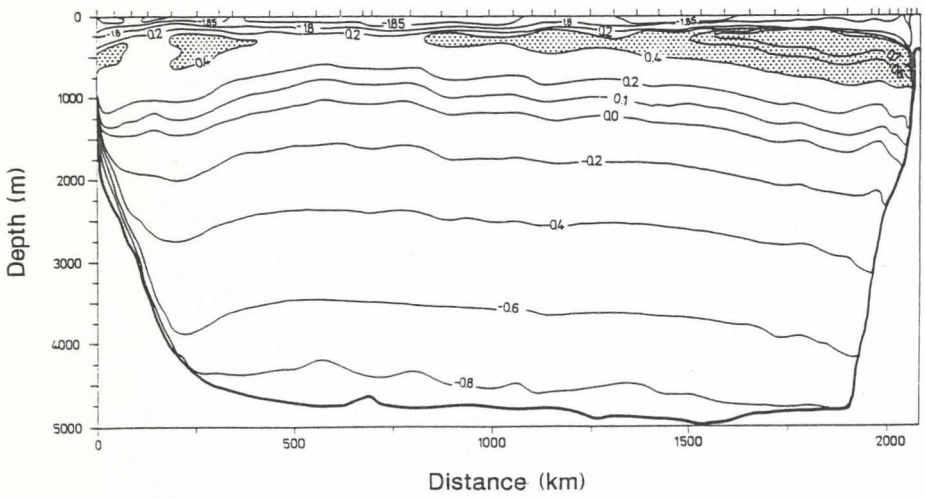

Figure 5: The section of temperature through the Weddell Sea in austral winter of 1989 (from the Winter Weddell Gyre Study 1989), at left the Antarctic Peninsula and at right Cape Norwegia on Antarctica. There is a break in the contour interval at $0.2°C$ to display the temperatures in the surface layer which are close to the freezing point (from Fahrbach et al. 1991).

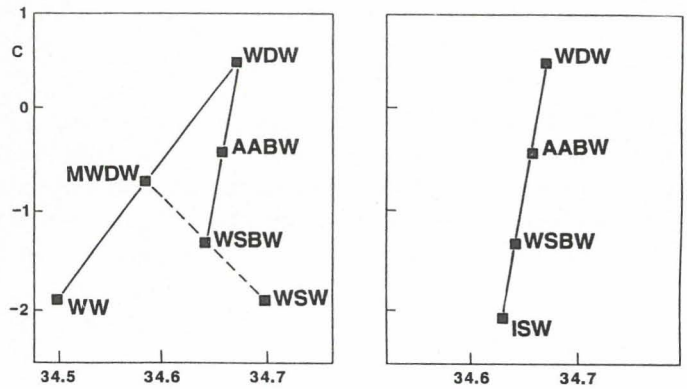

Figure 6: The mixing processes for production of $AABW$ in the T, S-diagram (from Fahrbach et al. 1992). Water masses are indicated by the squares, mixing path ways by lines connecting the squares. The left panel shows formations of $AABW$ through the Modified Warm Deep Water ($MWDW$) route (Foster and Carmack 1976), while the right panel shows the formation though the Ice Shelf Water (ISW) route (Foldvig et al. 1985a).

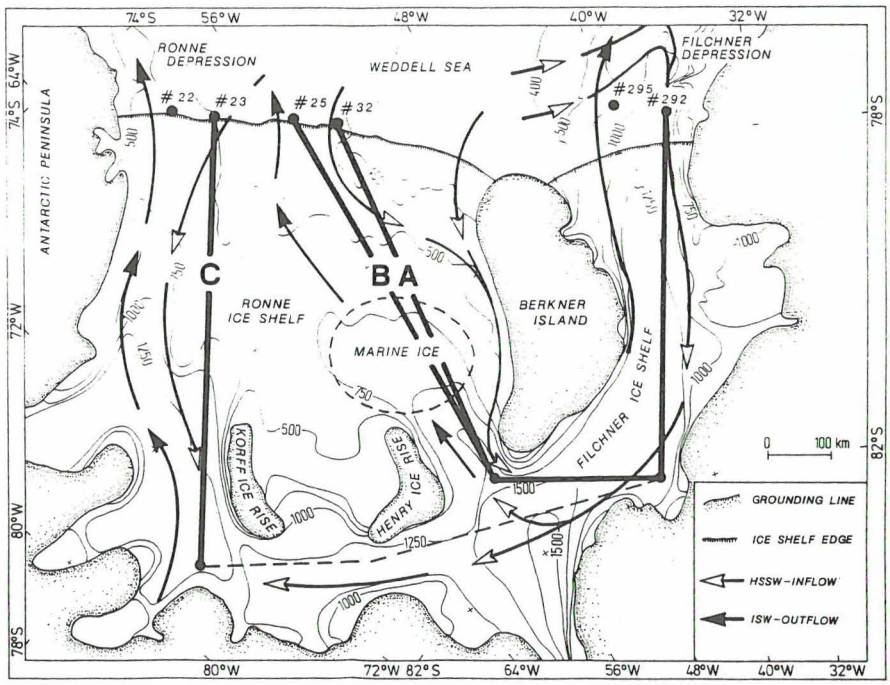

Figure 7: Map of the Filchner-Ronne Ice Shelf area, including the topography of ice bottom (in meters below sea level) and the possible paths of Western Shelf Water and Ice Shelf Water along the sections labeled A, B, and C. The location and numbers of the hydrographic stations used as boundary conditions for the model are indicated at the coast line.

was given by Robin (1979). He proposed that melting occurs at the grounding line and accumulation of ice near the ice shelf edge and related these processes to a single, essentially two-dimensional circulation regime. Hellmer and Olbers (1989) were the first to consider the full dynamical-thermodynamical implications of such a circulation cell in a two-dimensional model and revealed the essential interconnection of thermohaline processes at the ice shelf base and the sub-ice shelf circulation. Melting and freezing at the base of an ice shelf not only result from the sub-ice shelf circulation but also drive it and, more specifically, lead to the modification of the shelf water masses.

With reference to Hellmer and Olbers (1991) we discuss some results on the formation of *ISW* under the Filchner (*FIS*) and Ronne (*RIS*) Ice Shelves. *ISW* is observed in front of the *FIS* and can be traced from the ice shelf edge until it flows over a sill at the continental shelf break (Foldvig et al. 1985a,b) where it starts its mixing processes to produce *AABW* as desribed above. Two hypotheses are being discussed concerning the path of Western Shelf Water (*WSW*) which is the source water mass of *ISW*. This water mass originates from the freezing of sea ice along the coast of the western Weddell Sea. Its temperature is therefore at the freezing point (about $-1.86°C$) corresponding to surface pressure and salinity. *WSW* is observed to enter the *FIS* in the Filchner Depression east of Berkner Island (Robin et al. 1983). As an alternative path Foldvig et al. (1985a) have postulated that *WSW* enter on the western side of the island and flows under the *RIS* around to the Filchner side.

In any case the flow is driven under the ice by the thermohaline torque exerted by the temperature difference between the *WSW* at the front and the local freezing temperature at the shelf ice grounding line. The water comes in contact with the ice at the grounding line and is cooled and diluted by melting of basal ice. It creepes upward under the bottom of the shelf ice towards the front where it is expelled as the very cold *ISW*. If the water achieves local freezing temperature before the front is reached further pressure reduction will lead to super-cooling beyond the in-situ freezing point. This thermodynamic disequilibrium is compensated by the spontaneous formation of ice crystals in the water column and the accumulation of this marine ice under the ice shelf. Freezing rates of $1m/yr$ or higher may occur.

Hellmer and Olbers (1991) simulated the thermohaline circulation around Berkner Island with a 2-dimensional model for different vertical sections indicated on Figure 7. At the shelf ice front, temperature and salinity profiles are prescribed from observations (stations 22, 25, and 32 from Foldvig et al. 1985b, station 292 from Carmack and Foster 1975).

Though the paths under the RIS are only a few hundred km apart the circulation along them differs drastically (Figure 8). Along path A (Figure 8a) the *FIS* is dominated by an anticlockwise cell transporting warm and salty water near the bottom into the sub-ice cavity. It diverges at the deepest point of the section at the tip of Berkner Island, the major part flows back to the *FIS* side initiating the thermohaline scenario described above. A small branch supports a flow through the sub-ice channel towards the front on the *RIS*. Under the *RIS*, however, an internal cell arises which is essentially driven by an ice pump mechanism (Lewis and Perkin 1986): in the deeper part the ice melts and the diluted plume rises to lower pressures where freezing takes over, and the ice is indirectly pumped upwards. The circulation cell is driven by the re-supply of basal ice by the ice flow. Notice that water does not enter at the *RIS* front for path A. The meltwater plume which leaves there is modified *WSW* from the *FIS* side. The corresponding temperatures are displayed in Figure 8b. Path B gives only a slight variation of A.

The basic difference for path C (Figure 8c) is a slightly more saline bottom water at the *RIS* front (34.68 for C compared to 34.65 for A and 34.67 for B). Both regimes are dominated by cells of the same orientation but in C the transport of the *FIS*-cell is decreased by a factor of two and the *RIS*-cell is increased by a factor of four. The latter now transports bottom water from the *RIS* side into the interior and feeds the meltwater plumes of *ISW* on both sides of the Berkner Island.

Further investigation revealed that a critical salinity (for the present model version this is near 34.67) exists for the bottom layer at the *RIS* front which distinguishes between the two flow regimes shown here for the paths A (achieved for lower salinities) and C (achieved for higher salinities). They differ considerably with respect to their strength, their melting rates and of course also in their production rates and heat content of the resulting *ISW*. It is indeed conceivable that the seasonal cycle of ice freezing in the western shelf area of the Weddell Sea switches between the conditions of path A and path C.

4.2 An estimate of the formation rate of *AABW*

In view of the complex picture of *AABW* formation, we must realize that the route of reasoning for connections between the poleward heat transport and thermohaline processes in the remote areas around Antartica is full of side ways (we have not even considered open ocean convection) and paved with our lack of knowledge on many singles steps. Nevertheless, let us attempt to infer the formation rate of *AABW* from the model and mixing concept described above.

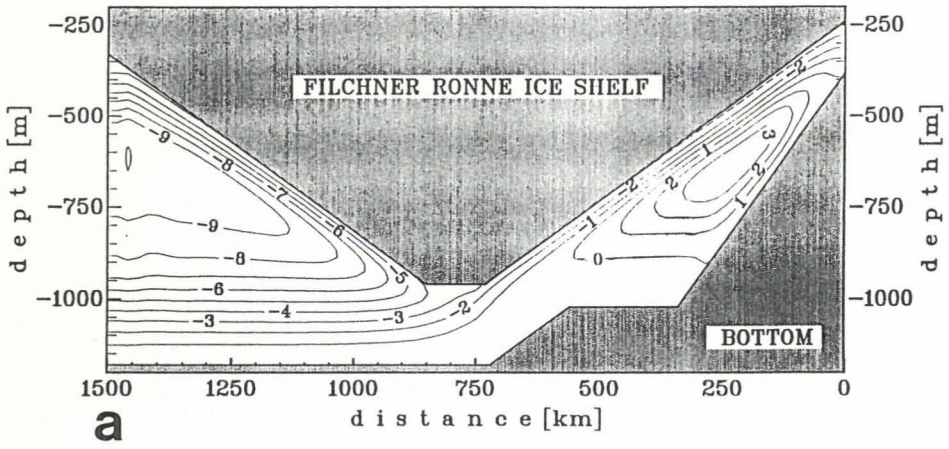
FILCHNER RONNE ICE SHELF
BOTTOM
depth [m]
distance [km]
-250
-500
-750
-1000
1500
1250
1000
750
500
250
0
-9
-8
-7
-6
-5
-4
-3
-2
-1
0
1
2
3

a

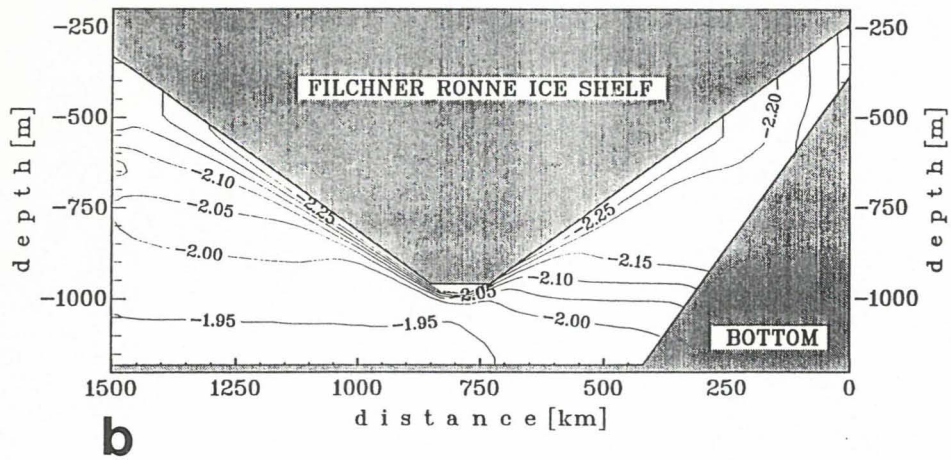
FILCHNER RONNE ICE SHELF
BOTTOM
depth [m]
distance [km]
-250
-500
-750
-1000
1500
1250
1000
750
500
250
0
-2.10
-2.05
-2.00
-1.95
-2.25
-2.20
-2.15

b

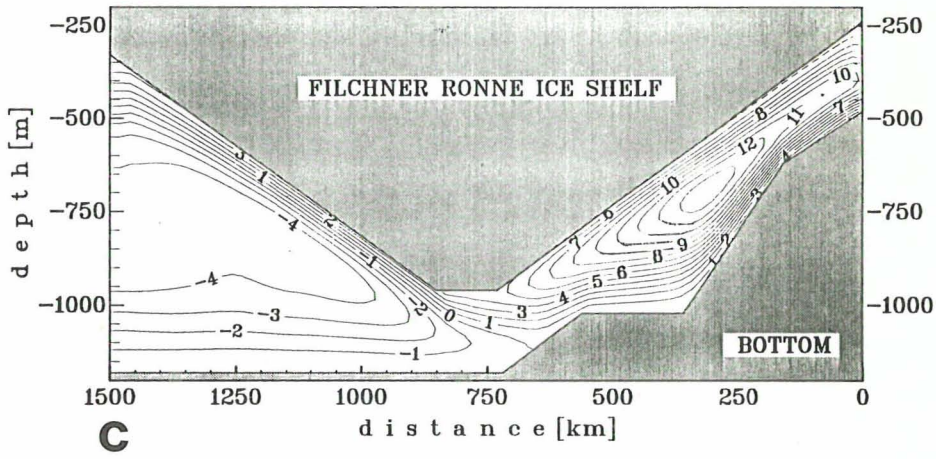

Figure 8: The flow beneath the Filcher-Ronne Ice Shelf for scenario A (top panel) with corresponding potential temperatures (middle panel) and the flow for scenario C (bottom panel). Contour interval of the streamfunction is $1m^2s^{-1}$, for temperature $0.05°C$.

In both circulation patterns under the shelf cavity the two-dimensional mass transport of *ISW* out of the *FIS* is $\approx 10m^2s^{-1}$, and, if multiplied by $120km$, the observed width of the *ISW* core on the western flank of the Filchner depression (Foldvig et al. 1985b) we arrive at about $1Sv$ for the rate of production of *ISW*. This agrees favourably with Foldvig et al. (1985a) who inferred the transport of *ISW* in the Filchner depression from current meter messurements.

Following now Foldvig's route $ISW + WDW \rightarrow WSBW$ and $WSBW + WDW \rightarrow AABW$ it is an easy matter to estimate the fraction of *ISW* in each parcel of *AABW* using either heat or salt conservation in this mixing scheme. Thus we find from the heat conservation equations

$$\begin{aligned} (1-\alpha)T_{ISW} + \alpha T_{WDW} &= T_{WSBW} \\ (1-\beta)T_{WSBW} + \beta T_{WDW} &= T_{AABW} \end{aligned} \tag{40}$$

that the basic members of the mixing process satisfy

$$(1-\alpha)(1-\beta)T_{ISW} + (\alpha(1-\beta)+\beta)T_{WDW} = T_{AABW} \tag{41}$$

With $T_{ISW} = -2.2°C, T_{WDW} = 0.5°C, T_{WSBW} = -1.2°C$ and $T_{AABW} = -0.4°C$ (mean values of the range in the Weddell Sea given by Foldvig et al. (1985a) and Carmack (1977)) we get $\alpha \approx 0.3$, $\beta \approx 0.5$ so that the fraction of *ISW* in *AABW* is given by $(1-\alpha)(1-\beta) \approx 0.35$.

Hence the formation rate of *AABW* in the Weddell Sea is approximately 3 times that of *ISW*. Following Carmack's (1977) estimate that only 70% of *AABW* is formed in this area we arrive, with a brave extrapolation, at a production rate of $5Sv$ for *AABW* from the *ISW*-route all around Antarctica. The formation process (Figure 6, left panel) involving Modified Warm Deep Water suggested by Foster and Carmack (1976) would add to this number. However, measurement of the level of the stable oxygen isotope O^{18} in *AABW* (Schlosser et al. 1990) indicates that the bottom water receives a significant fraction of meteoric melt water resulting from the melting of shelf ice. It is therefore believed that the *ISW*-route dominates the production of *AABW*. The value of $10Sv$ used for the transport of *AABW* across the Polar Front in chapter 2 can thus be seen as an upper limit.

5 Conclusions

The Southern Ocean is responsible for the cold climate of the present state of the world ocean. South of the Polar Front relatively warm water masses entering from northern oceans - mainly the Atlantic Ocean - are transformed to cold and heavy waters - notably the Antarctic Bottom Water - which spread northward and fill the bottom layers of the world ocean. The processes producing the cold deep water masses occur on small scales such as deep convection cells originating as a consequence of intricate thermohaline interaction of the ocean surface layer with the air and sea ice or with the the glacial ice at the bottom of the huge ice shelves around the Antarctic continent. The modification involves the mixing of various locally-produced water masses and others induced from remote areas. This process occurs on scales associated with the topography of the continental shelves and slopes. Also these scales are small compared to the broad ocean circulation.

The replenishment of heat for the Antarctic zone south of the Polar Front is mainly accomplished by eddy activity arising from instability processes of the Antarctic Circumpolar Current. Hence this important process is again operating on scales much smaller than the mean circulation itself. We have also shown that the heat flux is intimately related to the dynamical balance of the mean flow in which mesoscale eddies play a dominant role.

We have demonstrated that most of the above-mentioned processes can be simulated by suitably designed numerical models. In particular we have discussed results from an eddy resolving model of the circumpolar circulation in the Southern Ocean and from a model of the thermohaline induced circulation and water mass modification under the Filchner-Ronne Shelf Ice. Evidently a favourable comparison of model results with reality is mainly due to the adequate high resolution of each model, which was necessary to simulate the relevant processes on their intrinsic scales.

It also became evident that none of the processes in question could be resolved in any respect in the ocean components of the coarse climate models used today for investigating natural climate variabilty and man-made climate trends. The resolution of present coupled ocean-atmosphere models have a resolution of 4° to 6° in latitude and longitude (see e.g. Cubasch et al. 1992, Manabe et al. 1990) which is totally inadequate to implement eddy dynamics, convection, shelf and slope processes and even the thermohaline processes of air-ocean-ice interaction, all of which have a particular importance in the immediate region of the Southern Ocean as well as substantial influence on the rest of the world ocean.

References

BERGER, W. H., 1981: Paleoceanography: The deep-sea record. *In: The oceanic lithosphere The Sea Vol.* **7** (Ed. C. Emiliani), Wiley-Interscience, NY, pp. 1437-1519.

BRYAN, K., 1982: Poleward heat transport by the ocean. *Ann. Rev. Earth Planet. Sci.* , **10,** 15-38.

BRYDEN, H. L., 1983: The Southern Ocean. Eddies in Marine Science, A. R. Robinson, Ed., Springer, *265-277.*

CARMACK, E.C. AND T.D. FOSTER, 1975: Circulation and distribution of oceanographic properties near the Filchner Ice Shelf. *Deep-Sea Research,* **22,** 77-90.

CARMACK, E.C., 1986: Circulation and mixing in ice-covered waters. *In: Untersteiner, N. (Ed.), The geophysics of sea ice. NATO ASI Series B. Physics,* **Vol 146,** Plenum Publishing Corp., New York, 641-712.

CARMACK, E.C., 1977: Water characteristics of the Southern Ocean south of the Polar Front. In: *A voyage of Discovery (Ed. M. V. Angel), Pergamon Press, Oxford, 15-41.*

CUBASCH, U., HASSELMANN, K., HÖCK, H., MAIER-REIMER, E., MIKOLAJEWICZ, U., SANTER, B.D., AND R. SAUSEN 1991: Time-dependent Greenhouse warming computations with a coupled ocean-atmosphere model, 1992. *Climate Dyn.*,**8,** 55-69.

DESZOEKE, R. A., AND M. D. LEVINE, 1981: The advective flux of heat by mean geostrophic motions in the southern ocean. *Deep-Sea Res.,* **28,** 1057-1085.

ELIASSEN, A. AND E. PALM, 1961: On the transfer of energy in stationary mountain waves. *Geofys. Publ,* **22,** 1-23.

EMERY, W.L. AND J. MEINCKE, 1986: Global water masses: summary and review. *Oceanologica Acta,* **9,** 383-391.

FAHRBACH, E., M. KNOCHE AND G. ROHARDT, 1991: An estimate of water mass transformation in the southern Weddell Sea. *Marine Chemistry,* **35,** 25-44.

FAHRBACH, E., AUGSTEIN, E., AND D. OLBERS, 1992: Impact of shelf and sea ice on water mass modifications and large scale oceanic circulation in the Weddell Sea. *Subm. to Antartic Science–Global Concern, Conference Volume.*

FOLDVIK, A., T. GAMMELSRÖD AND T. TÖRRESEN, 1985A: Circulation and water masses on the southern Weddell Sea Shelf. *Antarctic Research Series,* **43,** 5-20.

FOLDVIK, A., T. GAMMELSRÖD, N. SLOTSVIK AND T. TÖRRESEN, 1985B: Oceanographic conditions on the Weddell Sea Shelf during the German Antarctic Expedition 1979/80. *Polar Research,* **3,** 209-226.

FOSTER, T. D., AND E. C. CARMACK, 1976: Frontal zone mixing and Antarctic Bottom Water formation in the southern Weddell Sea. *Deep-Sea-Res.* **23,** 301-317.

FRAM GROUP, 1991. An eddy-resolving model of the Southern Ocean. *EOS, 72,* **15,** 169-175.

GILL, A. E., 1968: A linear model of the Antarctic Circumpolar Current. *J. Fluid Mech.,* **32,** 465-488

GORDON, A.L. 1986: Interocean exchange of thermocline water. *J. Geophys. Res.,* **91,** 5037-5046.

GORDON, A. L., 1988: The Southern Ocean and global climate. *Oceanus* **31,** 39-46.

GORDON, A.L. AND W.B. OWENS, 1987: Polar Oceans. *Review of Geophysics*, **25**, 227-233.

HEIRTZLER, J.R. (ED.), 1985: Relief of the surface of the earth. *Rep. MGG-2, National Geophysical Data Center, Boulder, Colorado.*

HELLMER, H.H., AND D. OLBERS, 1989: A two-dimensional model for the thermohaline circulation under an ice shelf , *Antarctic Science* **1** , 325-336.

HELLMER, H.H., AND D.J. OLBERS, 1991: On the thermohaline circulation under the Filchner-Ronne Ice Shelf, *Antarctic Science*, **3**, 433-442.

HIDAKA, K., AND M. TSUCHIYA, 1953: On the Antarctic Circumpolar Current. *J. Mar. Res.*, **12**, 214-222

HOURY, S., E. DOMBROWSKY, P. DE MEY, AND J.-F. MINSTER, 1987: Brunt Väisälä frequency and Rossby radii in the Southern Ocean, *J. Phys. Oceanogr.*, **17**, 1619-1626.

JOHNSON, G. C. AND H. L. BRYDEN, 1989: On the size of the Antarctic Circumpolar Current. *Deep-Sea Res.*, **36**, 39-53.

LEVITUS, S., 1982 Climatological atlas of the world ocean. *NOAA Tech. Pap.* **3** , 173.

LEWIS, E. L., AND R. G. PERKIN, 1986: Ice pumps and their rates. *J. Geophys. Res.* **91**, 11756-11762.

MANABE, S., K. BRYAN AND M. J. SPELMAN, 1990: Transient response of a global ocean-atmosphere model to a doubling of atmopheric carbon dioxide. *J. Phys. Oceanogr.* **20**, 722-749.

MARSHALL, J., OLBERS, D. AND H. ROSS, 1993, Potential vorticity constraints on the dynamics and hydrography in the Southern Ocean. *J. Phys. Oceanogr., to appear.*

MCWILLIAMS, J. C., HOLLAND, W. R., CHOW, J. H. S., 1978: A description of numerical Antarctic Circumpolar Currents. *Dyn. Atmos. Oceans*, **2**, 213-291.

MUNK, W. H., AND E. PALMÉN, 1951: Note on the dynamics of the Antarctic Circumpolar Current . *Tellus*, **3**, 53-55.

NOWLIN JR., W.D. AND J.M. KLINCK, 1986 'The Physics of the Antarctic Circumpolar Current' *Reviews of Geophysics* **24**, 469-491.

OLBERS, D. J., AND M. WENZEL, 1989: Determining diffusivities from hydrographic data by inverse methods with applications to the circumpolar current. *Modelling the ocean general circulation and geochemical tracer transport. J. Willebrand and D. L. T. Anderson, Eds., NATO ASI Series C, Kluwer Acad. Publ.*, **284**, 95-122.

OLBERS, D., WÜBBER, CHR., AND J.-O. WOLF, 1993: The dynamical balance of wind and buoyancy driven circumpolar currents. *Submitted.*

RHINES, P.B., AND W.R. HOLLAND, 1979: A theoretical discussion of eddy-driven mean flows. *Dyn. Atmosph. Oceans* , **3**, 289-325.

ROBIN, G. DE Q., 1979: Formation, flow, and disintegration of ice shelves. *Journal of Glaciology*, **24** , 259-271.

ROBIN, G. DE Q., C.S.M. DOAKE, H. KOHNEN, R.D. CRABTREE, S.R. JORDAN AND D. MÖLLER, 1983: Regime of the Filchner-Ronne ice shelves, Antarctica.*Nature*,**302**, 582-586.

STEVENS, D.P., AND V.O.IVCHENKO, 1993: The zonal momentum balance in a realistic eddy resolving general circulation model of the Southern Ocean. *In preparation.*

SVERDRUP, H.U., 1940: Hydrology, Section II: Discussion. B.A.N.Z. Antarctic Research Expedition 1929-31, Reports-Ser. A, III, Oceanography, *Part 2, 88-126.*

TREGUIER, A. M., AND J. C. MCWILLIAMS, 1990: Topographic influences on wind-driven, stratified flow in β-plane channel: an idealized model for the Antarctic Circumpolar Current, *J. Phys. Oceanogr.*, **20,** 321-343.

WARRICK, R.A., AND H. OERLEMANS, 1990: Sea level rise. *In: Houghton, J.T. et al.(Eds), Climate change, the IPCC scientific assessment. University Press, Cambridge, 256-281.*

WHITWORTH III, T., 1988: The Antarctic Circumpolar Current. *Oceanus* **31,** 53-58.

WOLF-GLADROW, D., A. HENSE, J. SCHRÖTER AND D. OLBERS, 1993: A quasigeostrophic eddy-resolving model of the Antarctic Circumpolar Current, *In preparation.*

WOLFF, J.-O. AND D. OLBERS, 1989: The dynamical balance of the Antarctic Circumpolar Current studied with an eddy resolving quasigeostrophic model, *in: Mesoscale/synoptic coherent structures in geophysical turbulence, Ed. J. Nihoul, Elsevier Science Publ., 435-458.*

WOLFF, J.-O., E. MAIER-REIMER UND D.J. OLBERS, 1991: Wind-driven flow over topography in a zonal -plane channel: A quasigeostrophic model of the Antarctic Circumpolar Current, *J. Phys. Oceanogr.* **21,** 236-264

WORTHINGTON, L.V., 1981: The water masses of the world ocean: some results of a fine-scale census. *In: Warren, B,A., and C. Wunsch (Eds.): Evolution in physical oceanography. The MIT Press, Cambridge, 42-69.*